arXiv:1703.09249v1 [cond-mat.stat-mech] 27 Mar 2017

Physics of Mixed Reality

Ira B. Schwartz[1] and Klimka Szwaykowska[1] and Thomas W. Carr[2]
[1] *U.S. Naval Research Laboratory*
Code 6792, Plasma Physics Division, Nonlinear Systems Dynamics Section
Washington, D.C., 20375, USA
email:Ira.Schwartz@nrl.navy.mil
tel:202-404-8359 fax:202-767-0631
[2] *Department of Mathematics, Southern Methodist University, Dallas, Texas 75275, USA*
(Dated: March 29, 2017)

With the availability of ever more cheap and powerful computing, interest in the use of augmented and mixed-reality experiments has grown considerably in the engineering and physical sciences. Broadly speaking, these experiments consist of a simulated, or virtual model coupled directly to a physical experiment. Within the physical experiment, it is typical to find a good deal of uncertainty and noise since it is connected to the real world, and thus subjected to random perturbations. In contrast, the virtual part of the coupled system represents a somewhat idealized version of reality in which noise can be eliminated entirely, or at least well characertized. Thus, mixed-reality systems have very skewed sources of uncertainty spread through the entire system. In this paper, we consider a generic model of a mixed-reality system, and show how noise in the physical part of the system can influence the virtual dynamics through a large fluctuation, even when there is no noise in the virtual components. The virtual large fluctuation happens while the real dynamics exhibits only small random oscillations. We quantify the effects of uncertainty by showing how characteristic timescales of noise induced switching scale as a function of the coupling between the real and virtual parts of the experiment. Our results show that the probability of switching in the virtual world scales inversely as the square of reduced noise intensity amplitude, rendering the virtual probability of switching to be an *extremely rare event*. Our results are also confirmed through simulations, which agree quite well with analytic theory.

PACS numbers: 05.45.-a,05.40.-a,05.10.-a

I. INTRODUCTION

When exploring systems that consist of many communicating or coupled components, an increasingly large amount of effort is used to develop sophisticated real-time computer simulations of the interacting parts, without pairing interactively with real world experiments. Therefore, it is expected that large fluctuations due to noise will be missed. Swarms are an excellent model system where sophisticated models are used to predict behavioral patterns for large groups of interacting individual agents [1–4]. Validating the output of experiments and models is usually done after the simulated runs, with an attempt to account for uncertainties due to internal and external noise, as well as model uncertainties. That does not necessarily include data driven prediction, such as those used in short term weather forecasting [5–7], where uncertainty in the data and models may be considerable [8].

A mixed-reality (MR) experiment is one that combines real and simulated dynamical components, interacting through a hardware interface. A simple example of such a mixed-reality setup was demonstrated in [9], where the system consisted of two coupled horizontally driven pendulums, one of which was real, and the other simulated. Although more sophisticated models of friction were necessary to reproduce pendulum dynamics accurately in the simulation, it was shown that tuning the parameters of the virtual system can induce a transition from uncorrelated dynamics to a mixed reality state which is highly correlated. This example illustrates how exploration of a MR system can expose some of the uncertain modeling aspects, as well as noise effects of real world systems. Such analysis leads to better models in the end.

Another excellent example of how MR experiments can lead to better models is described in [10]. Here an experiment that was originally done with humans in the loop to create Bose-Einstein condensates was redone by replacing the humans with a machine learner. Removing the uncertainty using the learner showed an order of magnitude of increase in the production of condensates. The real experiment was now tied to a computer model reducing uncertainty, and rendering it an example of an MR system.

The science and engineering community has recently seen an impressive rise in MR experiments involving groups of autonomous mobile networked agents. Coordinated groups of agents have been deployed for a wide range of applications, including exploration and mapping of unknown environments [11–15], search and rescue [16, 17], and construction [18]. Extentions to the basic swarming dynamics by using teams of heterogeneous agents capable of cooperatively executing more complex tasks are presented in [19, 20]. In addition, network structure and uncertainties in delay communication have been shown to give rise to dynamic patterns in collective swarm motion [21, 22].

However, even as the complexity and sophistication

of cooperative robotic swarms in a structured environment has increased, the ability to perform reliable system validation in the presence of uncertainty remains a serious obstacle. Despite the accessibility of inexpensive small scale robotic platforms, experimental validation of many agent based systems still poses significant challenges. Many existing platforms must operate in indoor environments to reduce uncertainties, which limits the amount of available space for deployment of multilple agents simultaneously. As such, existing experiments are still typically performed using small numbers of actual robots, and large-scale experiments in artificial swarming are still largely conducted in simulation. This is unfortunate, because real-world testing always introduces a degree of noise and uncertainty that is difficult to accurately reproduce in a simulation setting.

In this paper we present a theoretical formulation of a mixed-reality setup for coupled systems in the presence of heterogeneous noise, where there is a large asymmetry between virual and real noise intensities. We show that even weak interaction between a low noise, or noise-free, simulated system and a noisy "real" system can cause catastrophic transitions between states. That is to say, even if only part of the system operates in noisy real-world conditions, we can observe large change in the dynamics of the idealized, low-noise virtual part. This is conceptually similar to the mixed-reality states observed in bidirectional coupling between real and simulated systems in [21].

One important aspect of the study of dynamical mixed-reality systems is the study of uncertainties and noise on the underlying deterministic dynamics [23, 24]. Although one might expect the deterministic dynamics would be only slightly perturbed in the presence of small noise, there are now many examples where noise causes a dramatic measurable change in behavior, such as noise-induced switching between attractors in continuous systems [25–31], and noise-induced extinction in finite-size systems [32–36].

In both switching and extinction, significant change in the state of the system occurs as the result of a large noise-induced fluctuation. For systems with small noise, such a fluctuation is a rare event, and occurs on average only when the noise signal lies along a so-called "optimal path" [37]. For systems operating in most common environments, noise is assumed to be homogeneous, and it is relatively straight-forward to compute the optimal paths which lead to large fluctuations [38]. However, for MR systems, the noise will have a large degree of heterogeneity between the real and simulated system components, due to large uncertainties in the dynamics of the real world and realtively smaller noise in the virtual world. The extreme case occurs in which there is no noise on the virtual dynamics, but a large fluctuation may occur nonetheless since noise is transmitted from the real to virtual world via coupling. In this limiting extreme case of heterogeneity, we will see how the large fluctuations come about. We refer to the state transitions induced in the noise-free virtual system by coupling with the noisy real-world system as extreme rare events.

The rest of the paper is laid out as follows. In section II we define the general asymmetric noise problem for MR systems. Gaussian noise is considered here, but the theory can be made more general to include non-Gaussian perturbations [39] and correlations [38, 40]. Noise induced large fluctuations are posed in a variational setting for the coupled problem. Linear response to the noise is derived in general. In section III, we consider a model problem of coupled bi-stable attractors subjected to asymmetric noise. For the specific problem we compare our theory to Monte Carlo simulations, and derive scalings as a function of the heterogeneity of the noise. We derive a general scaling relation between the noise ratio and the coupling strength that governs the mean probability to switch. To quantify the extreme rare event of virtual world switching, we derive the exponent of the probability distribution, and show that exponent varies as the inverse noise ratio squared. Comparisons between our general theory and numerical experiments of such large fluctuation events show excellent agreement.

II. PROBLEM SETUP IN GENERAL

The problem we consider begins when coupling virtual simulations with real physical dynamics, as shown in schematic in Fig. 1. Here we assume that the physical agents operate in a more uncertain, or noise-ridden, environment, which imposes a larger noise source on all of the agents. In contrast, the virtual world has much less uncertainty since it is isolated from any real environmental perturbations. We suppose that the time dependent vectors $\boldsymbol{x}, \boldsymbol{y}$ denote the state-space configurations of agents operating in virtual and real environments, respectively.

The basic premise we wish to examine occurs when the virtual world becomes ideal; i.e., given that the systems are coupled, how does real world noise affect the virtual dynamics when the latter's noise approaches zero.

A. The stochastic equations of motion

To analyze how noise impacts the dynamics from one environment to another, we consider a general coupled stochastic differential equation of the form

$$\dot{\boldsymbol{x}}(t) = \boldsymbol{f}(\boldsymbol{x}(t)) + \mathbf{h}_1(\boldsymbol{x}(t), \boldsymbol{y}(t), K) + \epsilon \boldsymbol{G}_1(\boldsymbol{x}(t))\boldsymbol{\xi}_{\boldsymbol{x}}(t), \tag{1}$$

$$\dot{\boldsymbol{y}}(t) = \boldsymbol{f}(\boldsymbol{y}(t)) + \mathbf{h}_2(\boldsymbol{x}(t), \boldsymbol{y}(t), K) + \boldsymbol{G}_2(\boldsymbol{y}(t))\boldsymbol{\xi}_{\boldsymbol{y}}(t), \tag{2}$$

where $\boldsymbol{x}, \boldsymbol{y} \in \mathbb{R}^n$ represent the physical quantities in state space as described above and the matrices $\boldsymbol{G}_i$, $i = 1, 2$ [41] are given by $\boldsymbol{G}_i(\boldsymbol{x}(t)) = \text{diag}\{g_{i1}(\boldsymbol{x}(t)), g_{i2}(\boldsymbol{x}(t)), ...g_{in}(\boldsymbol{x}(t))\}$, where the g_{ij}'s are general nonlinear functions. Coupling strength is denoted by parameter K, and we

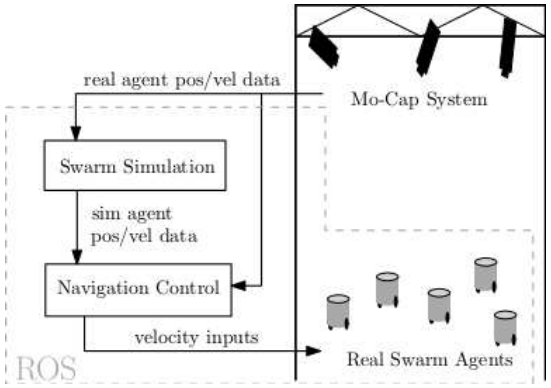

FIG. 1: Experimental setup with virtual swarm of agents. The real robots operate in a lab testbed. The positions of the real and simulated agents are passed to the virtual swarm simulator, which models the response of the virtual swarm agents to the current swarm configuration; and to the controller, which computes the real robot response and passes target velocities to the real swarm agents. Delay is introduced into the system artificially to simulate delays in real communication systems.

suppose $\mathbf{h}_1(\boldsymbol{x}(t), \boldsymbol{y}(t), 0) = \mathbf{h}_2(\boldsymbol{x}(t), \boldsymbol{y}(t), 0) = 0$; i.e., the systems $\boldsymbol{x}, \boldsymbol{y}$ are uncoupled when $K = 0$.

We assume that the noise inputs $\boldsymbol{\xi}_x, \boldsymbol{\xi}_y \in \mathbb{R}^n$ are independent, Gaussian-distributed stochatic processes with independent components, and intensity D. They are both characterized by a probability density functional $\mathcal{P}_{\boldsymbol{\xi}} = e^{-\mathcal{R}_\xi / D}$, where $\mathcal{R}_\xi$ is the *action*,

$$\mathcal{R}_{\boldsymbol{\xi}}[\boldsymbol{\xi}(t)] = \frac{1}{4} \int dt\, dt'\, \boldsymbol{\xi}(t) \boldsymbol{\xi}(t'). \tag{3}$$

In order to capture the asymmetric noise levels between the virtual and real worlds, we introduce a parameter, $\epsilon \ll 1$, that controls the noise intensity of the state variable $\boldsymbol{x}$. The case $\epsilon = 0$ corresponds to the virtual agent operating in a noise-free environment. However, noise-induced transitions in the virtual agent state can still occur as a result of noise tranferance through the coupling with the real agent.

B. Deterministic dynamics

In the absence of any noise, Eqs. 1, 2 are ordinary differential equations, and we suppose that there exist steady states which depend on the coupling strength, K. We therefore assume that there exists an attracting equilibrium, $(\boldsymbol{x}_a(K), \boldsymbol{y}_a(K))$, such that $\boldsymbol{x}_a(K) \neq \boldsymbol{y}_a(K)$. We also assume the existence of at least one saddle equilibrium point, $(\boldsymbol{x}_s(K), \boldsymbol{y}_s(K))$.

The stationary states satisfy.

$$\boldsymbol{f}(\boldsymbol{x}_a) + \mathbf{h}_1(\boldsymbol{x}_a, \boldsymbol{y}_a, K) = \boldsymbol{f}(\boldsymbol{x}_s) + \mathbf{h}_1(\boldsymbol{x}_s, \boldsymbol{y}_s, K) = 0 \tag{4}$$

$$\boldsymbol{f}(\boldsymbol{y}_a) + \mathbf{h}_2(\boldsymbol{x}_a, \boldsymbol{y}_a, K) = \boldsymbol{f}(\boldsymbol{y}_s) + \mathbf{h}_2(\boldsymbol{x}_s, \boldsymbol{y}_s, K) = 0. \tag{5}$$

The stability of the equilibrium states is given by the linear variational equations of motion about that state:

$$\dot{\mathbf{X}}(t) = \mathcal{M}(\bar{\boldsymbol{x}}, \bar{\boldsymbol{y}}, K)\mathbf{X}(t), \tag{6}$$

where $\bar{\boldsymbol{x}}, \bar{\boldsymbol{y}}$ denote either $\boldsymbol{x}_a, \boldsymbol{y}_a$ or $\boldsymbol{x}_s, \boldsymbol{y}_s$, and

$$\mathcal{M}(\bar{\boldsymbol{x}}, \bar{\boldsymbol{y}}, K) = \begin{bmatrix} \frac{\partial \mathbf{f}(\bar{\boldsymbol{x}})}{\partial x} + \frac{\partial \mathbf{h}_1(\bar{\boldsymbol{x}}, \bar{\boldsymbol{y}}, K)}{\partial x} & \frac{\partial \mathbf{h}_1(\bar{\boldsymbol{x}}, \bar{\boldsymbol{y}}, K)}{\partial y} \\ \frac{\partial \mathbf{h}_2(\bar{\boldsymbol{x}}, \bar{\boldsymbol{y}}, K)}{\partial x} & \frac{\partial \mathbf{f}(\bar{\boldsymbol{x}})}{\partial y} + \frac{\partial \mathbf{h}_1(\bar{\boldsymbol{x}}, \bar{\boldsymbol{y}}, K)}{\partial y} \end{bmatrix}$$

The matrix $\mathcal{M}(\bar{\boldsymbol{x}}, \bar{\boldsymbol{y}}, K)$ evaluated at the saddle point has only one positive real eigenvalue (associated with an unstable direction in the space of dynamical variables), while the rest of the eigenvalue spectrum lies in the left hand side of the complex plane. In particular we assume that for all values of interest K, the saddle point lies on the basin boundary of the attractor. If $K = 0$, we note that although (by assumption) $\boldsymbol{x}_a(0) \neq \boldsymbol{y}_a(0)$, they are still part of the same attractor.

When noise is added to the system, we wish to compute the probability of escaping from the basin of attraction of attractor $(\boldsymbol{x}_a, \boldsymbol{y}_a)$. The asymmetry of the noise between the virtual and real worlds is controlled by ϵ, which scales the noise intensity of $\boldsymbol{x}$. Computing the probability of escape in the small noise limit implies that we compute the most likely paths which cross the basin boundary of the attractor at the saddle point $(\boldsymbol{x}_s, \boldsymbol{y}_s)$. In describing the effect of how noise bleeds into the virtual world from the real world, we want to measure noise induced changes that are large in the dynamics of the $\boldsymbol{x}$ state while $\boldsymbol{y}$ remains approximately stationary; i.e., $\boldsymbol{y}$ does not change as much as $\boldsymbol{x}$. Thus, in the presense of noise we are interested in describing how the most likely path develops when $\boldsymbol{x}_a(K)$ changes its position much more than that of $\boldsymbol{y}_a(K)$. In the absence of noise and the system is uncoupled, we assume $\boldsymbol{x}_a(0)$ lies in a different part of phase than $\boldsymbol{y}_a(0)$. Therefore, we also assume that $||\boldsymbol{x}_a(K) - \boldsymbol{x}_s(K)|| \gg ||\boldsymbol{y}_a(K) - \boldsymbol{y}_s(K)||$, while $||\boldsymbol{y}_a(K) - \boldsymbol{y}_s(K)|| \ll 1$ given that the equilibria depend smoothly on the coupling strength K.

C. The Variational Formulation of Noise Induced Escape

For a given coupling K, we wish to determine the path with the maximum probability of noise induced switching from the initial attracting state $(\boldsymbol{x}_a(K), \boldsymbol{y}_a(K))$ to another attracting equilibrium $(\boldsymbol{x}_b(K), \boldsymbol{y}_b(K))$, where the initial and final states are equilibria of the noise-free version equations given by zeros of Eqns. 5. Each attractor possesses its own basin of attraction, and therefore on

average, small noise is expected to induce small fluctuations about the stable equilibria. However, sometimes the noise will organize itself in such a way that a large fluctuation occurs, allowing escape over the effective energy barrier away from the stable equilibrium. If the fluctuation is sufficiently large to bring the system state close to the saddle point, there is a possibility of switching. Near the saddle point, depending on the sign of the projection of the local trajectory onto the unstable manifold of the positive eigenvalue, the system will approach one or the other attractor. Switching occurs once the trajectory enters a different basin of attraction from the one where it started.

We assume the noise intensity D is much smaller than the effective barrier height, and the parameter $0 \leq \epsilon < 1$. Note also that noise terms (ξ_x, ξ_y) are formally the time derivative of a Brownian motion, sometimes referred to as white noise [42].

For D sufficiently small, we make the ansatz that the probability distribution of observing such a large fluctuation scales exponentially as the inverse of D [25, 38],

$$\mathcal{P}_x = e^{-R/D}, \tag{7}$$

where

$$R(K) = \min_{(\boldsymbol{x},\boldsymbol{y},\boldsymbol{\xi}_x,\boldsymbol{\xi}_y,\boldsymbol{\lambda_1},\boldsymbol{\lambda_2})} \mathcal{R}(\boldsymbol{x},\boldsymbol{y},\boldsymbol{\xi}_x,\boldsymbol{\xi}_y,\boldsymbol{\lambda_1},\boldsymbol{\lambda_2};K), \tag{8}$$

and

$$\begin{aligned}\mathcal{R}(\boldsymbol{x},\boldsymbol{\xi},\boldsymbol{y},\boldsymbol{\xi},\boldsymbol{\lambda_1},\boldsymbol{\lambda_2};K) &= R_{\xi_x}[\boldsymbol{\xi}_x(t)] + R_{\xi_y}[\boldsymbol{\xi}_y(t)] \\ &+ \int_{-\infty}^{\infty} dt \boldsymbol{\lambda_1}(t)\cdot[\dot{\boldsymbol{x}}(t) - \boldsymbol{f}(\boldsymbol{x}(t)) - \mathbf{h}_1(\boldsymbol{x}(t),\boldsymbol{y}(t),K) - \epsilon \boldsymbol{G}_1(\boldsymbol{x}(t))\xi_{\mathbf{x}}(t)] \\ &+ \int_{-\infty}^{\infty} dt \boldsymbol{\lambda_2}(t)\cdot[\dot{\boldsymbol{y}}(t) - \boldsymbol{f}(\boldsymbol{y}(t)) - \mathbf{h}_2(\boldsymbol{x}(t),\boldsymbol{y}(t),K) - \boldsymbol{G}_2(\boldsymbol{y}(t))\boldsymbol{\xi_y}(t)].\end{aligned} \tag{9}$$

We will see later that the Lagrange multipliers, $\boldsymbol{\lambda}_1, \boldsymbol{\lambda}_2$, also correspond to the conjugate momenta of the equivalent Hamilton-Jacobi formulation of this problem [43]. Similar to classical mechanics, the exponent R of Eq. 7 is called the action, and corresponds to the minimizer of the action in the Hamilton-Jacobi formulation which occurs along the optimal path. This path will minimize the integral of Eq. 9, and is found by setting the variations along the path $\delta\mathcal{R}$ to zero. The transition rate exponent is proportional to the action, R.

When computing the action, the boundary conditions are important, especially since in general they depend the parameters of the problem Therefore, we suppose that dynamics starts near the attractor $(\boldsymbol{x}_a, \boldsymbol{y}_a)$. Small fluctuations will on average remain in the basin of the attractor until at some point in time, the dynamics hits the saddle point, $(\boldsymbol{x}_s, \boldsymbol{y}_s)$. Thus, we have the boundary conditions given by:

$$\lim_{t\to-\infty}(\boldsymbol{x}(t),\boldsymbol{y}(t)) = (\boldsymbol{x}_a(K),\boldsymbol{y}_a(K)) \tag{10}$$

$$\lim_{t\to\infty}(\boldsymbol{x}(t),\boldsymbol{y}(t)) = (\boldsymbol{x}_s(K),\boldsymbol{y}_s(K)). \tag{11}$$

To examine the structure of the Hamiltonian governing the large fluctuations, we take the variational derivative of $\mathcal{R}(\boldsymbol{x},\boldsymbol{\xi},\boldsymbol{y},\boldsymbol{\xi},\boldsymbol{\lambda_1},\boldsymbol{\lambda_2};K)$ with respect to the noise sources, $\boldsymbol{\xi}_i$ (where $i = \boldsymbol{x},\boldsymbol{y}$). Setting the derivative equal to 0 gives

$$\boldsymbol{\xi_x} = 2\epsilon \boldsymbol{G}_1(\boldsymbol{x})\boldsymbol{\lambda}_1 \tag{12}$$

$$\boldsymbol{\xi_y} = 2\boldsymbol{G}_2(\boldsymbol{y})\boldsymbol{\lambda}_2. \tag{13}$$

The full set of equations of motion is then derived by taking the variational derivatives with respect to the state variables and their corresponding momenta:

$$\begin{aligned}\dot{\boldsymbol{x}} &= \boldsymbol{f}(\boldsymbol{x}) + \mathbf{h}_1(\boldsymbol{x},\boldsymbol{y},K) + 2\epsilon^2 \boldsymbol{G}_{\mathbf{1}}^2(\boldsymbol{x})\boldsymbol{\lambda}_1 \\ \dot{\boldsymbol{\lambda}}_1 &= -\epsilon^2 \boldsymbol{G_1}(\boldsymbol{x})\frac{\partial \boldsymbol{G_1}(\boldsymbol{x})}{\partial \boldsymbol{x}}\boldsymbol{\lambda}_1\boldsymbol{\lambda}_1 - \frac{\partial(\boldsymbol{f}(\boldsymbol{x}) + \mathbf{h}_1(\boldsymbol{x},\boldsymbol{y},K))}{\partial \boldsymbol{x}}\boldsymbol{\lambda}_1 \\ &\quad - \frac{\partial(\mathbf{h}_2(\boldsymbol{x},\boldsymbol{y},K))}{\partial \boldsymbol{x}}\boldsymbol{\lambda}_2 \\ \dot{\boldsymbol{y}} &= \boldsymbol{f}(\boldsymbol{y}) + \mathbf{h}_2(\boldsymbol{x},\boldsymbol{y},K) + 2\boldsymbol{G}_{\mathbf{2}}^2(\boldsymbol{y})\boldsymbol{\lambda}_2 \\ \dot{\boldsymbol{\lambda}}_2 &= -\boldsymbol{G_2}(\boldsymbol{y})\frac{\partial \boldsymbol{G_2}(\boldsymbol{y})}{\partial \boldsymbol{y}}\boldsymbol{\lambda}_2\boldsymbol{\lambda}_2 - \frac{\partial(\boldsymbol{f}(\boldsymbol{y}) + \mathbf{h}_2(\boldsymbol{x},\boldsymbol{y},K))}{\partial \boldsymbol{y}}\boldsymbol{\lambda}_2 \\ &\quad - \frac{\partial(\mathbf{h}_1(\boldsymbol{x},\boldsymbol{y},K))}{\partial \boldsymbol{y}}\boldsymbol{\lambda}_1.\end{aligned} \tag{14}$$

The full Hamiltonian is derived by substituting the ansatz in Eq. 7 into the appropriate Fokker-Planck equation and dropping terms or order higher than $1/D$, which results in a Hamilton-Jacobi equation with Hamiltonian:

$$\begin{aligned}H &= [\epsilon^2 \boldsymbol{G}_{\mathbf{1}}^2(\boldsymbol{x})\boldsymbol{\lambda}_1]\cdot\boldsymbol{\lambda}_1 + [\boldsymbol{G}_{\mathbf{2}}^2(\boldsymbol{y})\boldsymbol{\lambda}_2]\cdot\boldsymbol{\lambda}_2 \\ &\quad + \boldsymbol{\lambda}_1\cdot[\boldsymbol{f}(\boldsymbol{x}) + \mathbf{h}_1(\boldsymbol{x},\boldsymbol{y},K)] \\ &\quad + \boldsymbol{\lambda}_2\cdot[\boldsymbol{f}(\boldsymbol{y}) + \mathbf{h}_2(\boldsymbol{x},\boldsymbol{y},K)].\end{aligned} \tag{15}$$

One immediate observation from Eqn. 14 is that from the conjugate variables, $(\boldsymbol{\lambda}_1, \boldsymbol{\lambda}_2) \equiv (\mathbf{0}, \mathbf{0})$ is an invariant manifold. Moreover, for the system to remain at the equilibria, in Eq. 14, the conjugate variables must vanish. (Here, we assume that multiplicative noise functions do

not vanish at the equilibria.) Although the action is in the exponent of the distribution, the conjugate momenta act as an effective control force that pushes the system along a most likely path from the attractor to the saddle point. From Eqns. 12 and 13, it is therefore clear that the noise must be related to a large fluctuation governed by the conjugate variables in the system. Since at the equilibrium points of the attractor or saddle, the noise does not contribute to the exponent of the distribution, we assume that the other boundary conditions at equilibrium points for $\boldsymbol{\lambda}_i$ are

$$\lim_{t\to\pm\infty}(\boldsymbol{\lambda}_1(t),\boldsymbol{\lambda}_2(t)) = (\mathbf{0},\mathbf{0}). \tag{16}$$

Locating and computing the most likely, or optimal, path for basin escape revolves around computing the solution to the two point boundary value problem consisting of Eqns. 14 and boundary conditions 16 and 11. However, one must check the local stability of the equilibria at the boundaries. It can be shown that if the attractor and saddle points in the deterministic system have nonzero real parts of the their linear spectra, then the full set of conservative equations of motion will have saddle points at the boundaries. That is, both the deterministic attractors and saddles will appear as saddles in the Hamiltonian formulation. A fairly general proof in finite dimensions as well as a useful general method of computing the solutions for the optimal path can be found in [44].

Finally, we note that once we have the optimal path satisfying the variational problem above, the switching rate from one attractor to the other is given to logarithmic accuracy by

$$W = C\exp(-\frac{R}{D}), \tag{17}$$

where C is a constant and R is given by Eq. 8.

D. Perturbation of Variation

Because the optimal-path equations are in general nonlinear, solving them analytically is unrealistic. However, in the case where the coupling constant K is small, we can use perturbation theory, assuming that the variational trajectories remain close to the corresponding trajectories for $K = 0$. Even though the measured perturbation terms will be small, they affect the exponent of the distribution, and since the action is divided by a small intensity, D, even a small change in the action could have a large effect on the density and mean switching times.

Assuming the terms in the vector field of Eq. 14 are sufficiently smooth, we suppose the coupling terms $(\mathbf{h}_1(\boldsymbol{x},\boldsymbol{y},K),\mathbf{h}_2(\boldsymbol{x},\boldsymbol{y},K))$ may be expanded in terms of K as:

$$\mathbf{h}_1(\boldsymbol{x},\boldsymbol{y},K) = K\hat{\mathbf{h}}_1(\boldsymbol{x},\boldsymbol{y}) + O(K^2) \tag{18}$$

$$\mathbf{h}_2(\boldsymbol{x},\boldsymbol{y},K) = K\hat{\mathbf{h}}_2(\boldsymbol{x},\boldsymbol{y}) + O(K^2). \tag{19}$$

Using Eq. 19, we may be rewrite the the action to first order in K:

$$\begin{aligned}\mathcal{R}(\boldsymbol{x},\boldsymbol{\xi},\boldsymbol{y},\boldsymbol{\xi},\boldsymbol{\lambda_1},\boldsymbol{\lambda_2};K) = \mathcal{R}_0(\boldsymbol{x},\boldsymbol{\xi},\boldsymbol{y},\boldsymbol{\xi},\boldsymbol{\lambda_1},\boldsymbol{\lambda_2}) \\ + K\mathcal{R}_1(\boldsymbol{x},\boldsymbol{\xi},\boldsymbol{y},\boldsymbol{\xi},\boldsymbol{\lambda_1},\boldsymbol{\lambda_2})\end{aligned} \tag{20}$$

where

$$\mathcal{R}_0(\boldsymbol{x},\boldsymbol{\xi_x},\boldsymbol{y},\boldsymbol{\xi_y},\boldsymbol{\lambda_1},\boldsymbol{\lambda_2}) = R_{\xi_x}[\boldsymbol{\xi}_x(t)] + R_{\xi_y}[\boldsymbol{\xi}_y(t)] \tag{21}$$

$$+ \int_{-\infty}^{\infty} dt\boldsymbol{\lambda_1}(t)\cdot[\dot{\boldsymbol{x}}(t) - \boldsymbol{f}(\boldsymbol{x}(t)) - \epsilon\boldsymbol{G}_1(\boldsymbol{x}(t))\xi_{\mathbf{x}}(t)] \tag{22}$$

$$+ \int_{-\infty}^{\infty} dt\boldsymbol{\lambda_2}(t)\cdot[\dot{\boldsymbol{y}}(t) - \boldsymbol{f}(\boldsymbol{y}(t)) - \boldsymbol{G}_2(\boldsymbol{y}(t))\boldsymbol{\xi_y}(t)] \tag{23}$$

and

$$\begin{aligned}\mathcal{R}_1(\boldsymbol{x},\boldsymbol{\xi_x},\boldsymbol{y},\boldsymbol{\xi_x},\boldsymbol{\lambda_1},\boldsymbol{\lambda_2}) = \\ - \int_{-\infty}^{\infty} dt[\boldsymbol{\lambda_1}(t)\cdot\hat{\mathbf{h}}_1(\boldsymbol{x}(t),\boldsymbol{y}(t)) \\ + \boldsymbol{\lambda_2}(t)\cdot\hat{\mathbf{h}}_2(\boldsymbol{x}(t),\boldsymbol{y}(t))].\end{aligned} \tag{24}$$

The first order correction to the action can be found by first finding the solution that minimizes the action to $\mathcal{R}_0(\boldsymbol{x},\boldsymbol{\xi_x},\boldsymbol{y},\boldsymbol{\xi_y},\boldsymbol{\lambda_1},\boldsymbol{\lambda_2})$ and is denoted by $(\boldsymbol{x}^0,\boldsymbol{\xi}^0_{\boldsymbol{x}},\boldsymbol{y}^0,\boldsymbol{\xi}^0_{\boldsymbol{y}},\boldsymbol{\lambda}^0_{\mathbf{1}},\boldsymbol{\lambda}^0_{\mathbf{2}})$. Then we evaluate the integral explicitly in Eq. 24 at the zeroth order minimization. We note that higher order terms may be found by applying standard perturbation theory to the equations of motion and boundary conditions directly, or we may use the general distribution theory [45] to get the next order in K, which we do below.

The Hamiltonian for the variation of the action $\mathcal{R}_0$ of the uncoupled system is given by

$$\begin{aligned}H^0 = \epsilon^2[\boldsymbol{G}^2_{\mathbf{1}}(\boldsymbol{x}^0)\boldsymbol{\lambda}^0_1]\cdot\boldsymbol{\lambda}^0_1 + [\boldsymbol{G}^2_{\mathbf{2}}(\boldsymbol{y}^0)\boldsymbol{\lambda}^0_2]\cdot\boldsymbol{\lambda}^0_2 \\ + \boldsymbol{\lambda}^0_1\cdot\boldsymbol{f}(\boldsymbol{x}^0) + \boldsymbol{\lambda}^0_2\cdot\boldsymbol{f}(\boldsymbol{y}^0).\end{aligned} \tag{25}$$

The structure of Eq. 25 is such that the total action is just the sum of the action of the $\boldsymbol{x}$ and $\boldsymbol{y}$ variables since $K = 0$. In addition the initial and final states for $K = 0$ are given for the attractor $(\boldsymbol{x}_a^0, \boldsymbol{y}_a^0)$ and saddle $(\boldsymbol{x}_s^0, \boldsymbol{y}_s^0)$. Since we are interested in moving $\boldsymbol{x}$ through a large fluctuation while holding $\boldsymbol{y}$ approximately constant, when uncoupled the initial states satisfy $\boldsymbol{x}_a^0 \neq \boldsymbol{y}_a^0$, while $\boldsymbol{y}_s^0 = \boldsymbol{y}_a^0$, the latter assuming no movement in $\boldsymbol{y}$.

The effect of the noise reducing parameter on the action is now evident from the equations of motion derived from Eq. 25. The total action is just the sum of the $\boldsymbol{x}$ and $\boldsymbol{y}$ actions, $\mathcal{R}^0[\boldsymbol{x}], \mathcal{R}^0[\boldsymbol{y}]$, respectively. Moreover, since the there is no movement in $\boldsymbol{y}$, $\mathcal{R}^0[\boldsymbol{y}] \equiv 0$. Assuming the multiplicative noise term is non-singular, the resulting uncoupled action is therefore given by

$$\mathcal{R}^0[\boldsymbol{x}] = -\frac{1}{\epsilon^2}\int_{\boldsymbol{x}_A}^{\boldsymbol{x}_s} [\boldsymbol{G}_1^2]^{-1}\boldsymbol{f}(\boldsymbol{x})d\boldsymbol{x}. \tag{26}$$

The expected effect of the parameter ϵ is evident, in that the action scales as $\frac{1}{\epsilon^2}$. Coupled with the fact that the action is in exponent of the distribution means that the exponent should scale as $\frac{1}{\epsilon^2 D}$, which will make the probability of $\boldsymbol{x}$ transitioning through a large fluctuation conditioned on $\boldsymbol{y}$ staying approximately constant a very rare event.

Notice that we can also consider how $\boldsymbol{y}$ switches while keeping $\boldsymbol{x}$ within a basin by constraining its motion. Here the switching rate is much higher since the exponent of the switching rate scales just as $\frac{1}{D}$.

To see how such a rare event explicitly comes about, we consider the following generic bi-stable situation.

III. A MODEL EXAMPLE OF MIXED REALITY NOISE INDUCED PERTURBATIONS

For clarity, we now give an example of noise-induced switching in a generic coupled system where the individual components are affected by different scales of noise. Consider two coupled particles interacting in a double-well potential $U(x)$. One particle represents a simulated robotic agent, while the other represents the real-world robot that interacts with the simulation. The two-particle system is used because it is sufficiently complex to illustrate our argument, while remaining simple enough to be understood. Our approach follows the general theory of switching in the previous section, but for purposes of analysis we consider the following symmetric double-well potential:

$$U(x) = \frac{x^4}{4} - \frac{x^2}{2}. \tag{27}$$

In the absence of coupling, the resulting motion of a single particle is described by $\frac{\mathrm{d}x}{\mathrm{d}t} = f(x) = -\frac{dU(x)}{dx}$. Now suppose that the (x, y) particles are coupled with a spring potential [21], and a white Gaussian noise ξ_x, ξ_y is assumed to act on each particle independently. Let x and y denote the positions of particles 1 and 2, respectively. Their equations of motion are then:

$$\dot{x} = f(x) - K(x - y) + \epsilon\xi_x \tag{28a}$$
$$\dot{y} = f(y) + K(x - y) + \xi_y. \tag{28b}$$

We assume that $E[\xi_x(s)\xi_y(t)] = 2D\delta(t-s)\delta(x-y)$, where $D \ll 1$ is the noise intensity, and ϵ the satisfies the hypotheses in the previous section.

A. The deterministic picture

Consider the noise-free system obtained by setting $\xi_x \equiv 0, \xi_y \equiv 0$ in (28). The system has as its full potential a function $V(x, y; K)$ given by:

$$V(x, y, K) = -1/2\,x^2 + 1/4\,x^4 - 1/2\,y^2 + 1/4\,y^4 + 1/2\,K\,(x - y)^2 \tag{29}$$

The topology of the equilibria for $K = 0.1$ is pictured in Fig. 2.

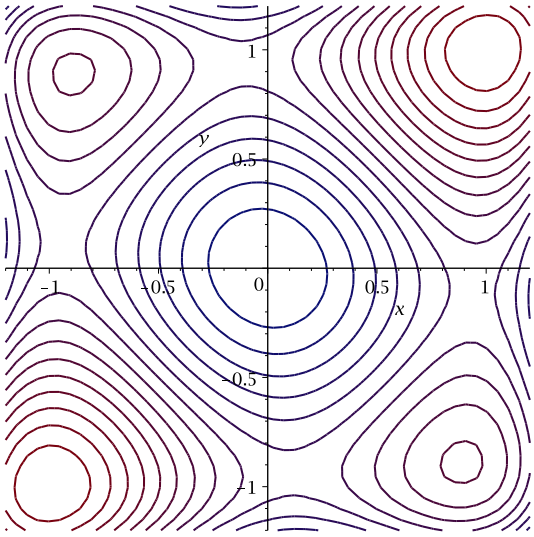

FIG. 2: (Color) A contour plot of the potential function $V(x, y; 0.1)$.

The system has stable equilibria at $(x, y) = (\pm 1, \pm 1)$. The equilibrium solution $(x, y) = (0, 0)$ is unstable for $K < 1/2$ and a saddle point for $K > 1/2$. The symmetric configuration about 0, with $(x, y) = (\pm\sqrt{1-2K}, \mp\sqrt{1-2K})$, is stable for $K \in [0, 1/3)$ and a saddle for $K \in (1/3, 1/2]$ (note, this solution does not exist for $K > 1/2$).

The system has 4 additional equilibria, defined by

$$(x, y) = (\zeta, \frac{\zeta}{K}(\zeta^2 + K - 1)) \tag{30}$$

where ζ is a root of

$$\zeta^4 + (K - 1)\zeta^2 + K^2 = 0. \tag{31}$$

Solutions exist for $K \in [0, 1/3]$; the corresponding equilibria are saddle points. A plot of values of ζ for different K is shown in Fig. 3.

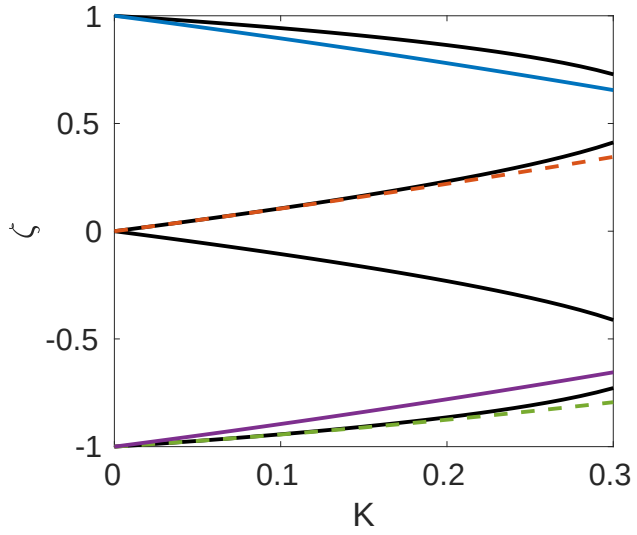

FIG. 3: (Color) Values of zeroes of the deterministic vector field as a function of the coupling strength K. Gray lines denotes solutions to the exact expression in Eq. 30. Dashed lines denote the asymptotic approximate equilibria for small K: saddle ($\boldsymbol{x}_S$,red,$\boldsymbol{y}_S$,green). Solid thick lines denote the asymptotic branch of attractors ($\boldsymbol{x}_A$,blue,$\boldsymbol{y}_A$,purple).

Since we are interested in having the particles start at different phase space positions, we examine small K asymptotics using perturbation theory. The initial attractor is at $(\boldsymbol{x}_a(K), \boldsymbol{y}_a(K)) \approx (1 - K - K^2/2, -1 + K + K^2/2)$; i.e., we have the particles start in different parts of phase space. The final point prior to switching is to have the dynamics get to the saddle on the basin boundary. Here the saddle point is given by $(\boldsymbol{x}_s(K), \boldsymbol{y}_s(K)) \approx (K + K^2/2, -1 + 2K + 5K^2/8)$. Notice that where noise will force x will move a distance of order unity, y will move only order K, where $K \ll 1$. An example of a path of such a conditioned dynamics is shown in Fig. 4.

Before proceeding to the full noise case, we note that when $K = 0$, the origin is a repeller; i.e., it is not a saddle. However, when we add coupling, the origin becomes a saddle point

B. Switching

When adding noise into the system, it is possible to observe noise-induced switching between stable equilibria of the noise-free system. For sufficiently small noise intensity D, the switching dynamics can be described using the Hamiltonian formulation of Eq. 14, where we extend

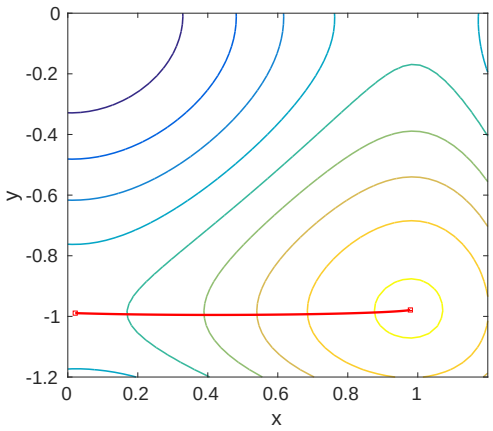

FIG. 4: (Color) The potential function Eq. 29 for $K = 0.0209$ for the zero noise case. Overlaid is the predicted optimal path (red line) computed when $\epsilon = \frac{1}{2}$. For the boundary conditions chosen, x starts near 1 and goes through a large fluctuation, while y remains approximately stationary near -1.

the system to 4 dimemsions by adding in conjugate momenta (λ_1 and λ_2), and set the multiplicative noise terms to the identity:

$$\dot{x} = f(x) - K(x - y) + 2\epsilon^2\lambda_1 \tag{32a}$$
$$\dot{y} = f(y) + K(x - y) + 2\lambda_2 \tag{32b}$$
$$\dot{\lambda}_1 = -(f'(x) - K)\lambda_1 - K\lambda_2 \tag{32c}$$
$$\dot{\lambda}_2 = -(f'(y) - K)\lambda_2 - K\lambda_1, \tag{32d}$$

with corresponding Hamiltonian

$$\mathcal{H}(x, y, \lambda_1, \lambda_2) = [f(x) - K(x - y)]\lambda_1 + [f(y) + K(x - y)]\lambda_2 + \lambda_2^2 + \epsilon^2\lambda_1^2. \tag{33}$$

Note that $\mathcal{H}(x^*, y^*, 0, 0) = 0$ for all (x^*, y^*) in the set of equilibria of (28). Since $\mathcal{H}$ is time-invariant, optimal switching paths between equilibria are required to satisfy a two-point boundary problem on the zero level-sets of $\mathcal{H} = 0$ in order to compute the action.

Suppose that for $t \to -\infty$, x and y start in a symmetric configuration $(x, y) = (\sqrt{1 - 2K}, -\sqrt{1 - 2K})$. We are interested in the optimal switching path which causes both particles to end up in a single well, at $x = y = -1$. In the small noise limit, we know that given a path starting at the attractor, it must pass through a basin boundary saddle point. Therefore, we use the numerical approach described in [44], and compute the optimal path to the saddle point given by $(\zeta, \frac{\zeta}{K}(\zeta^2 + K - 1))$ as $t \to \infty$, where $1/\sqrt{3} < \zeta < 1$.

In Eqns. 32, consider the limit $K \to 0$. The particle motions are uncoupled, and the situation is equivalent to a single-particle switching problem. In this case, it is possible to find an analytic solution in time explicitly, and make use of the general perturbation theory. From

Eq. 26, we know that for non-zero ϵ, the zeroth order term of the action scales inversely with ϵ^2, and in fact is given by

$$R^0 = \frac{1}{4\epsilon^2}, \tag{34}$$

where we have used the fact that from the Hamiltonian, the optimal path when $K = 0$ is given explicitly by $\lambda_1^0 = -\frac{1}{\epsilon^2} f(x^0)$.

To get the first order corrections, we need the solution to the two point value problem along the zeroth order optimal path as a function of time:

$$x^0(t) = \frac{1}{\sqrt{1+e^{2t}}} \tag{35a}$$
$$y^0(t) = -1 \tag{35b}$$
$$\lambda_1^0(t) = -\frac{\mathrm{e}^{2\,t}}{\left(1+\mathrm{e}^{2\,t}\right)^{3/2}\,\epsilon^2} \tag{35c}$$
$$\lambda_2^0(t) = 0 \tag{35d}$$

Notice that as $t \to \pm\infty$, we have the following boundary conditions satisfied for $(x^0(t), \lambda_1^0(t))$ while holding $(y^0 \equiv -1, \lambda_2^0 = 0)$ constant:

$$\lim_{t\to-\infty} \qquad \lim_{t\to\infty} \tag{36a}$$
$$x^0(t) \to x_a^0 = 1 \qquad x^0(t) \to x_s^0 = 0 \tag{36b}$$
$$\lambda_1^0(t) \to 0 \qquad \lambda_1^0(t) \to 0. \tag{36c}$$

Using the zeroth order time series in the first order expression of the action gives to linear order in K

$$\mathcal{R} = \frac{1}{4\epsilon^2} - K\frac{3}{2\epsilon^2}. \tag{37}$$

C. Second order effects

We can get the second order terms in K to the action by considering the potential function of Eq. 29, and using the general results of computing the probability of escape for Gaussian noise in (boucher et al). However, the approach here is one that will be problem specific. We choose to formally examine the Hamiltonian in Eq. 33, and notice that y and its conjugate momenta remain approximately near the attractor. Therefore, we use the asymptotic expression of the attractor and saddle, in the limits of Eq. 24.

$$\begin{aligned}\mathcal{R}_1 &= \int_{-\infty}^{\infty} dt[\boldsymbol{\lambda_1}(t)\cdot\hat{\mathbf{h}}_1(\boldsymbol{x}(t),\boldsymbol{y}(t)) \\ &\qquad + \boldsymbol{\lambda_2}(t)\cdot\hat{\mathbf{h}}_2(\boldsymbol{x}(t),\boldsymbol{y}(t))] \\ &= -\int_{-\infty}^{\infty} dt\frac{f(x_0(t)}{\epsilon^2}(x_0(t)-y_0(t)) \\ &= \frac{1}{\epsilon^2}\int_{x_A(K)}^{x_s(K)} dx_0(x_0+1)\end{aligned} \tag{38}$$

Using the asymptotic expressions for the attractor and saddle for x_0, expanding for small K, and collecting terms, we have formally that

$$\mathcal{R} \approx \frac{1}{4\epsilon^2} - \frac{3K}{2\epsilon^2} + \frac{2K^2}{\epsilon^2}. \tag{39}$$

An example of the optimal path projections is given in Fig. 5 for moderate noise reduction of ϵ and small coupling K. Notice that in the figure, $(x(t), y(t))$ spend most of their time near the equilibria specified at the boundaries. In addition, $x(t)$ traverses a distance of order unity when it switches from the attractor to the saddle point, while $y(t)$ traverses only by an order of K. Therefore, even though the scaled reduction of the noise parameter is small, the noise transmitted to x has a very strong effect through the coupling strength K.

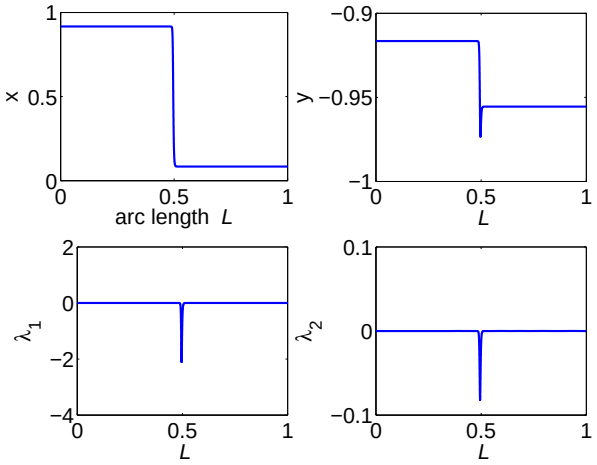

FIG. 5: (Color) Trajectory projections of the optimal path where time is rescaled to be arc length, L, along the trajectory. Shown are trajectories for x, y and their conjugate variables λ_1, λ_2. The parameters used are $\epsilon = 0.5, K = 0.08$.

Using the theory for the action, Fig. 6 shows how it scales as a function of K when $\epsilon \approx 0.5$. Along with the computed action are the results from the asymptotic analysis for small coupling using Eq. 39. Notice that for $K < 0.2$, the agreement is good, and improves as K gets smaller.

One of the interesting facets of the problem occurs when there is noise only on the y component, and zero noise on x. This situation occurs when ϵ approaches zero. Although asymptotically the action is seen to approach ∞ as ϵ approaches zero, since the system is coupled it is possible to compute an optimal path conditioned on that large fluctuations occur only in x. Using the results for finite ϵ as an initial guess, we use continuation to decrease ϵ to 0, and obtain the optimal path for switching in the coupled system with noise acting only on particle y (see Fig. 7), where the coupling constant is relatively small; i.e. $K \approx 0.06$. The action along the optimal path is on

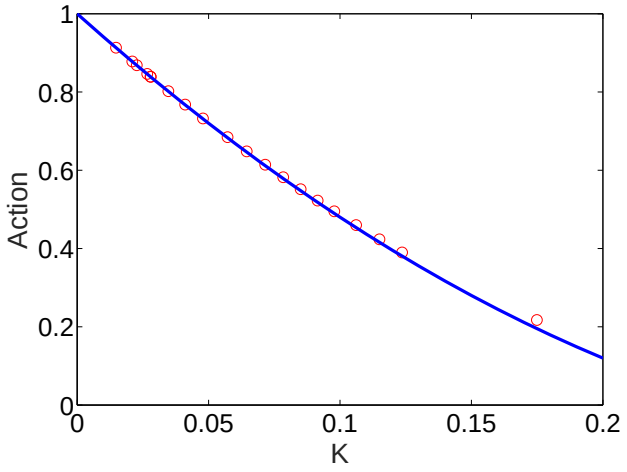

FIG. 6: (Color) The computed action (red circles) plotted as a function of coupling parameter K, $\epsilon \approx 0.5$. The asymptotic result for small K using Eq. 39 is shown (Blue curve)

.

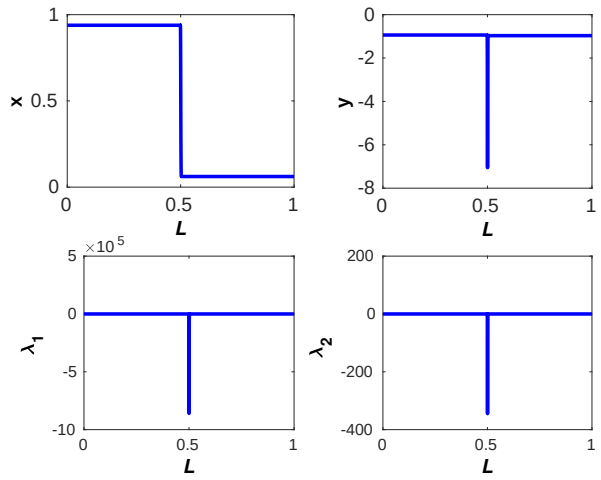

FIG. 7: (Color) Optimal switching path for the system in (32), with $K = 0.0595$ and $\epsilon = 0$ to machine precision.

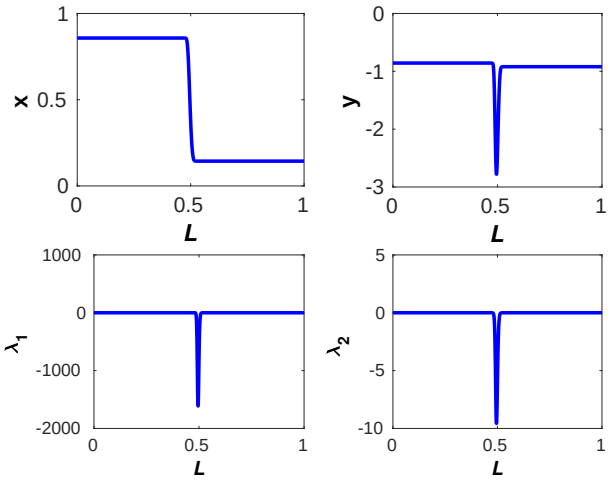

FIG. 8: (Color) Trajectory projections of the optimal path where time is rescaled to be arc length, L, along the trajectory. Shown are trajectories for x, y and their conjugate variables λ_1, λ_2. The parameters used are $\epsilon = 0.0, K = 0.1324$.

the order of 10^5, which indicates that switching would be an extremely rare event. We do however, get a relatively large change in y which is on the order of unity instead of K, but y does spend most its time near its equilibria.

The interaction of the coupling on the noise induced forces is essential. If we increase the coupling K by an order of magnitude, we have a drastic change in the conjugate variables, as shown in Fig. 8. Here we see that x still undergoes a change of order unity, and y does as well. However, the biggest change is in the size of the relative fluctuations corresponding to the conjugate variables λ_1, λ_2, which have been reduced by several orders of magnitude. The action is therefore much smaller and is given by $\mathcal{R} \approx 500$, implying a much shorter switching time when the coupling is weak, which is given by $\mathcal{R} \approx 5.7 \cdot 10^5$.

In summary, we show a plot of the asymptotic scaling of the action varying ϵ over an order of magnitude in Fig. 9. Here one observes that the range of K for which the asymptotic prediction of the action holds decrease as ϵ decreases.

D. Monte Carlo Simulation

We consider the problem of switching in Eqs. 28 where the asymmetry in noise intensity between two coupled systems is governed by the parameter ϵ. Using the Milstein method, we implement a Monte Carlo scheme to compute the mean time for the x variable to switch while the y variable remains in its basin, given that the particles start in different basins of attraction. That is, we compute the mean time it takes for x to transition from $x(0) = x_A(K)$ to the saddle point $x(T) = x_S(K)$.

We first check the existence of an exponential distribution of times by computing the switching time as a function of the inverse noise intensity for various values of ϵ and K. From the ansatz that the mean switching time exponents are proportional to $\mathcal{R}/D$, we plot the log of the mean switching time as a function of $1/D$, where the slope should be the action evaluated at the parameters of ϵ, K.

We can see how the asymptotic theory holds as a function of K by comparing it with the mean switching times in Fig. 11. For small K, the theory holds up quite well for a range of noise intensities small compared to the barrier

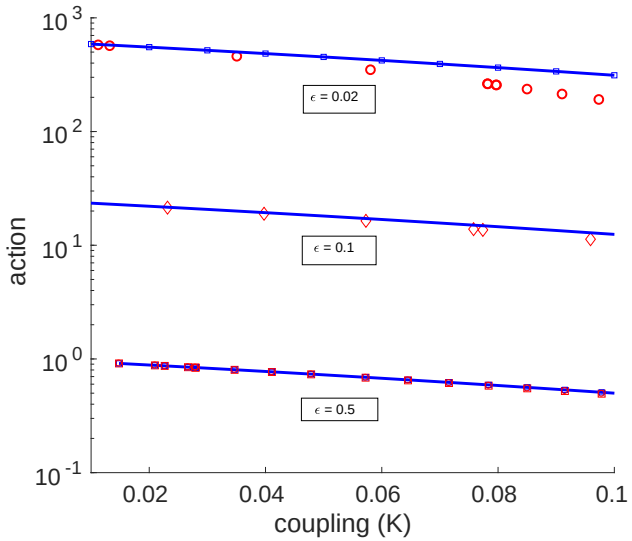

FIG. 9: (Color) A plot showing the computed log of the action and the asymptotic approximation (Eq. 39) as a function of coupling strength, K. Shown are results for $\epsilon = 0.5, 0.1, 0.02$. The computed action is represented by red squares, triangles and circles, while the asymptotic expression is depicted as blue lines.

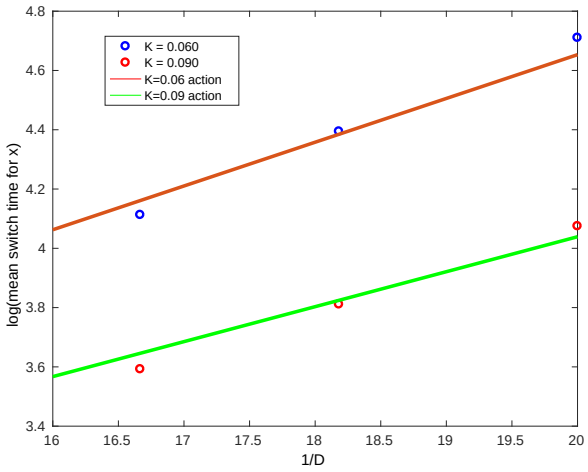

FIG. 10: (Color) Plotted is the mean switching time for x to go from the attractor to the saddle point while y remains in its basin of attraction. Here $\epsilon = 0.75$. The Monte Carlo simulations are in circles while the theory of the action was computed using Eq. 32 and the boundary conditions.

height, and over sufficiently large range of K.

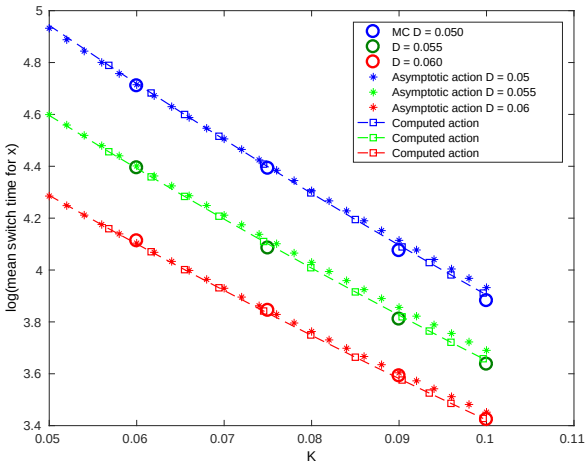

FIG. 11: (Color) Plotted is the mean switching time for x as a function of K. Here $\epsilon = 0.75$. The Monte Carlo simulations are in circles while the theory of the action was computed using asymptotic theory of Eq. 39. We note that the theory (asterisks) is good up to a pre-factor of the switching times, and the theory was shifted to coincide with the first data point. In addition, the actual computed action is shown as dashed lines so that the difference between theory and computation for large K values is evident.

IV. DISCUSSION AND CONCLUSION

We considered the problem of mixed-reality systems, which consist of coupled virtual and real dynamics. Since the dynamics of real platforms is exposed to uncertain environments, our models considered highly heterogeneous noise distributions in which the virtual dynamics had considerably less noise than the real dynamics.

As an example of a MR system, we ran a preliminary experiment of a delay coupled swarm of $N-1$ virtual agents, which were mutually coupled to a single real agent. The bifurcation structure is predicted theoretically in [46], and a description of a swarm experiment is given in [21]. The laws of motion followed by both real and virtual agents in the experiment are described by the following equations, which are dimensionalized versions of the equations of motion in [46]:

$$\ddot{\mathbf{r}}_i = \beta\left(v_0^2 - \dot{\mathbf{r}}_i^2\right)\dot{\mathbf{r}}_i - \frac{\alpha}{N}\sum_{\substack{j=1\\ i\neq j}}^{N}(\mathbf{r}_i(t) - \mathbf{r}_j(t-\tau)), \qquad (40)$$

$$i = 1, 2 \ldots, N, \qquad (41)$$

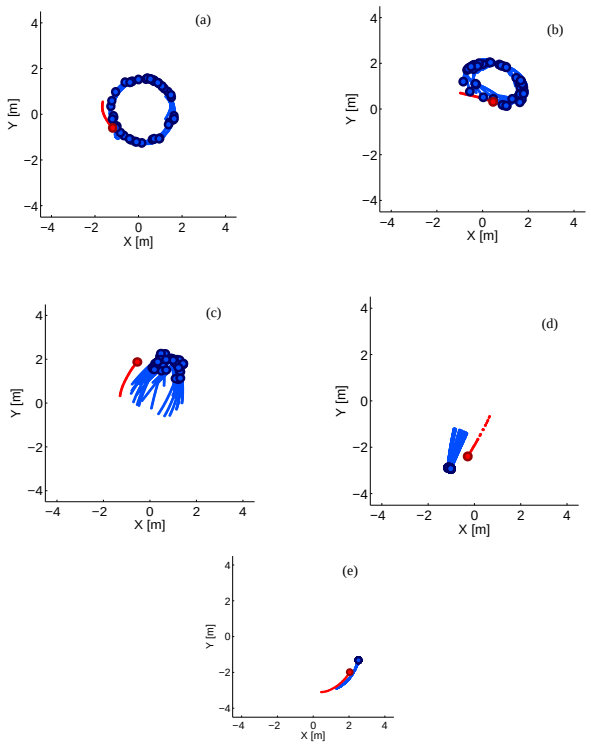

FIG. 12: (Color) Time snapshots of a delay coupled mixed-reality experiment plot position of virtual agents (blue) and the real agent (red). The ring state parameters used: $\tau = 2.0s, \alpha = 0.0826/s^2, \beta = 1.0m/s^2, v_0 = 0.2m/s$. The rotating parameters used: $\tau = 20.0s, \alpha = 0.05/s^2, \beta = 1.0m/s^2, v_0 = 0.2m/s$. There is no repulsion force on the virtual agents, so that in panel (e) they all may lie on top of one another.

where the units of α, β and v_0 are as follows:

$$[\alpha] = \frac{1}{\text{time}^2},$$
$$[\beta] = \frac{\text{time}}{\text{length}^2},$$
$$[v_0] = \frac{\text{length}}{\text{time}}.$$

Swarm dynamic patterns are govered by the time delay τ in the communication between agents. Depending on the length of the delay, the overall swarm exhibits one of two basic dynamical patterns. One is a *ring state*, in which the agents revolve around a stationary center of mass. As delay in increased, the system undergoes a Hopf bifurcation and the system converges to a *rotating state*, in which the center of mass of the agents rotates about a stationary point.

In the experiment, the delay was tuned initially so that the swarm converged to the ring state, and then turned past the bifurcation at a random time. The time snapshots shown in Fig. 12 show a switch in which the entire swarm of virtual and real agents move from the ring state to a rotating state.

When more real agents are added to the mix, the impact of uncertain perturbations and noise through the coupling mechansim on the virtual agents becomes significant, and may itself cause a random change in the virtual dynamics, as predicted by our generic switching theory.

The theoretical problem we addressed was whether the effect of coupling was sufficient to cause the virtual dynamics to undergo a large fluctuation while the real dynamics, which was driven by larger noise intensity, remained quiescent. It was very natural to take a variational approach to describing such a large fluctuation, and although it was applied to Gaussian noise, it can be extended to more general noise sources [47].

Using the variational approach, we generated a Hamiltonian two-point boundary value problem with asymmetric driving representing the effect of the heterogeneous noise sources. The solution to these equations generates the optimal switching path, which in turn can be used to predict mean escape rates. Here we showed just how the optimal path reveals a large fluctuation in the virtual dynamics while the real dynamics remains in its local basin. Note that since the noise level in the real system is significantly higher, the probability of a noise-induced transition occuring in this system before the virtual one is high. Thus the previous situation of having the virtual dynamics switch first is an extreme rare event.

We then used the general theory on a model coupled system of a pair of particles in a bi-stable potential. This was similar to experiments modeled by swarming agents [21]. For a given noise intensity D, the scale parameter ϵ was used to quantify the asymmetry of noise distribution. We then quantified the action as a function of coupling strength over a larger range of ϵ, revealing an excellent comparison between asymptotic theory and numerical solutions of the optimal paths. We further quantified the mean escape times in terms of parameters ϵ and D, again with excellent agreement between simulation and theory for the log of the mean switching time.

Finally, we note we computed the paths as the noise fraction ϵ approaches zero, so that the probability of extremely rare events was governed by coupling strength alone. That is, the noise is only transmitted through the coupling terms. The asymptotic theory predicts an logarithmic exponent of the probability of virtual switching given that the real dynamics exhibits only small fluctuations, where the exponent scales as $1/\epsilon^2$. Although extremely rare, the switching is still observed when coupling is sufficiently large. [48]

V. ACKNOWLEDGMENTS

The authors gratefully acknowledge the Office of Naval Research for their support under N0001412WX20083, and support of the NRL Base Research Program

N0001412WX30002. KS was a National Research post doctoral fellow while performing the research. We acknowledge useful conversations with Ani Hsieh, Luis Mier, and Brandon Lindley about early versions of the research, and Jason Hindes for an initial reading of the mansucript. We also thank Nitin Sydney and Don Sofge for sharing the results of the preliminary mixed reality swarm experiment at NRL.

[1] Eshel Ben-Jacob, Inon Cohen, András Czirók, Tamás Vicsek, and David L. Gutnick, "Chemomodulation of cellular movement, collective formation of vortices by swarming bacteria, and colonial development," Physica A **238**, 181–197 (1997).

[2] Daniel S. Calovi, Ugo Lopez, Sandrine Ngo, Clement Sire, Hugues Chaté, and Guy Theraulaz, "Swarming, schooling, milling: Phase diagram of a data-driven fish school model," New Journal of Physics **16**, 015026 (2014), arXiv:1308.2889.

[3] E. Carlen, R. Chatelin, P. Degond, and B. Wennberg, "Kinetic hierarchy and propagation of chaos in biological swarm models," Physica D: Nonlinear Phenomena **260**, 90–111 (2013).

[4] M. Ani Hsieh, Ádám Halász, Spring Berman, and Vijay Kumar, "Biologically inspired redistribution of a swarm of robots among multiple sites," Swarm Intelligence **2**, 121–141 (2008).

[5] Steven J Greybush, Eugenia Kalnay, Takemasa Miyoshi, Kayo Ide, and Brian R Hunt, "Balance and ensemble kalman filter localization techniques," Monthly Weather Review **139**, 511–522 (2011).

[6] L. Kuznetsov, Kayo Ide, and Christopher K. R. T. Jones, "A method for assimilation of lagrangian data," Monthly Weather Review **131**, 2247–2260 (2003).

[7] Pierre F. J. Lermusiaux, "Data assimilation via error subspace statistical estimation. part II: Middle Atlantic Bight shelfbreak front simulations and ESSE validation," Monthly Weather Review **127**, 1408–1432 (1999).

[8] T. N. Palmer, "Predicting uncertainty in forecasts of weather and climate," Reports on Progress in Physics **63**, 71–116 (2000).

[9] Vadas Gintautas and Alfred W. Hübler, "Experimental evidence for mixed reality states in an interreality system." Physical Review E **75**, 057201 (2007).

[10] P. B. et al. Wigley, "Fast machine-learning online optimization of ultra-cold-atom experiments." Sci. Rep. **6**, 25890 (2016).

[11] E.J.P. Earon, T.D. Barfoot, and G.M.T. D'Eleuterio, "Development of a multiagent robotic system with application to space exploration," (2001) pp. 1267–1272, IEEE/ASME International Conference on Advanced Intelligent Mechatronics.

[12] Chayan Benerjee and Navya Deepthi, "Multiagent Coalition Formation for Distributed Area Coverage & Exploration," (2015) pp. 1–6, International Conference on Robotics, Automation, Control and Embedded Systems.

[13] Subhrajit Bhattacharya, Robert Ghrist, and Vijay Kumar, "Multi-robot Coverage and Exploration on Riemannian Manifolds with Boundary," International Journal of Robotics Research **33**, 113–137 (2012).

[14] Kevin M. Lynch, Ira B. Schwartz, Peng Yang, and Randy A. Freeman, "Decentralized Environmental Modeling by Mobile Sensor Networks," IEEE Transactions on Robotics **24**, 710–724 (2008).

[15] Wencen Wu and Fumin Zhang, "Cooperative exploration of level surfaces of three dimensional scalar fields," Automatica **47**, 2044–2051 (2011).

[16] R. Takano, D. Yamazaki, Y. Ichikawa, K. Hattori, and K. Takadama, "Multiagent-based ABC algorithm for Autonomous Rescue Agent Cooperation," (2014) pp. 585 – 590, IEEE International Conference on Systems, Man and Cybernetics.

[17] Hend Al Tair, Tarek Taha, Mahmoud Al-Qutayri, and Jorge Dias, "Decentralized Multi-agent POMDPs Framework for Humans-Robots Teamwork Coordination in Search and Rescue," (2015) pp. 210–213, International Conference on Information and Communication Technology Research.

[18] Frederico Augugliaro, Sergei Lupashin, Michael Hamer, Cason Male, Markus Hehn, Mark W. Mueller, Jan Sebastian Willmann, Fabio Gramazio, Matthias Kohler, and Raffaello D'Andrea, "The flight assembled architecture installation: Cooperative contruction with flying machines," IEEE Control Systems **34**, 46–64 (2014).

[19] S. R. Ramp, Russ E. Davis, Naomi Ehrich Leonard, I. Shulman, Yi Chao, A. R. Robinson, Jerrold E. Marsden, Pierre F. J. Lermusiaux, David M. Fratantoni, J. D. Paduan, F. P. Chavez, F. L. Bahr, S. Liang, W. Leslie, and Z. Li, "Preparing to predict: the second autonomous ocean sampling network (AOSN-II) experiment in the Monterey Bay," Deep Sea Research Part II: Topical Studies in Oceanography **56**, 68–

[20] Marco Dorigo, Dario Floreano, Luca Maria Gambardella, Francesco Mondada, Stefano Nolfi, Tarek Baaboura, Mauro Birattari, Michael Bonani, Manuele Brambilla, Arne Brutschy, Daniel Burnier, Alexandre Campo, Anders Lyhne Christensen, Antal Decugniere, Gianni Di Caro, Frederick Ducatelle, Eliseo Ferrante, Alexander Forster, Javier Martinez Gonzales, Jerome Guzzi, Valentin Longchamp, Stephane Magnenat, Nithin Mathews, Marco Montes de Oca, Rehan O'Grady, Carlo Pinciroli, Giovanni Pini, Philippe Retornaz, James Roberts, Valerio Sperati, Timothy Stirling, Alessandro Stranieri, Thomas Stutzle, Vito Trianni, Elio Tuci, Ali Emre Turgut, and Florian Vaussard, "Swarmanoid: A Novel Concept for the Study of Heterogeneous Robotic Swarms," IEEE Robotics & Automation Magazine **20**, 60–71 (2013).

[21] Klementyna Szwaykowska, Ira B Schwartz, Luis Mier-y-Teran Romero, Christoffer R Heckman, Dan Mox, and M Ani Hsieh, "Collective motion patterns of swarms with delay coupling: Theory and experiment," Physical Review E **93**, 032307 (2016).

[22] Jason Hindes, Klementyna Szwaykowska, and Ira B. Schwartz, "Hybrid dynamics in delay-coupled swarms with "mothership" networks," PHYSICAL REVIEW E **94**, 032306 (2016).

[23] C. W. Gardiner, Handbook of Stochastic Methods for Physics, Chemistry and the Natural Sciences (Springer-Verlag, 2004).

[24] N. G. Van Kampen, Stochastic Processes in Physics and Chemistry (Elsevier, 2007).

[25] M. I. Freidlin and A. D. Wentzell, Random Perturbations of Dynamical Systems (Springer-Verlag, 1984).

[26] M. G. Castellano, G. Torrioli, C. Cosmelli, A. Costantini, F. Chiarello, P. Carelli, G. Rotoli, M. Cirillo, and R. L. Kautz, "Thermally activated escape from the zero-voltage state in long josephson junctions," Phys. Rev. B **54**, 15417–15428 (1996).

[27] H. B. Chan and C. Stambaugh, "Activation barrier scaling and crossover for noise-induced switching in micromechanical parametric oscillators," Phys. Rev. Lett. **99**, 060601 (2007).

[28] C. R. Doering and J. C. Gadoua, "Resonant activation over a fluctuating barrier," Phys. Rev. Lett. **69**, 2318–2321 (1992).

[29] Jeffrey Emenheiser, Airlie Chapman, Marton Posfai, James P. Crutchfield, Mehran Mesbahi, and Raissa M. D'Souza, "Patterns of patterns of synchronization: Noise induced attractor switching in rings of coupled nonlinear oscillators," CHAOS **26** (2016), 10.1063/1.4960191.

[30] Otti D'Huys, Thomas Juengling, and Wolfgang Kinzel, "Stochastic switching in delay-coupled oscillators," PHYSICAL REVIEW E **90** (2014), 10.1103/PhysRevE.90.032918.

[31] M. I. Dykman and I. B. Schwartz, "Large rare fluctuations in systems with delayed dissipation," PHYSICAL REVIEW E **86** (2012), 10.1103/PhysRevE.86.031147.

[32] Jason Hindes and Ira B. Schwartz, "Epidemic extinction and control in heterogeneous networks," Phys. Rev. Lett. **117**, 028302 (2016).

[33] A. Kamenev, B. Meerson, and B. Shklovskii, "How colored environmental noise affects population extinction," Phys. Rev. Lett. **101**, 268103 (2008).

[34] Alex Kamenev and Baruch Meerson, "Extinction of an infectious disease: A large fluctuation in a nonequilibrium system," Phys. Rev. E **77**, 061107 (2008).

[35] Mark I. Dykman, Ira B. Schwartz, and Alexandra S. Landsman, "Disease extinction in the presence of random vaccination," Phys. Rev. Lett. **101**, 078101 (2008).

[36] Daniel K. Wells, William L. Kath, and Adilson E. Motter, "Control of Stochastic and Induced Switching in Biophysical Networks," PHYSICAL REVIEW X **5** (2015), 10.1103/PhysRevX.5.031036.

[37] I.B. Schwartz, E. Forgoston, S. Bianco, and L.B. Shaw, "Converging towards the optimal path to extinction," Journal of The Royal Society Interface **8**, 1699–1707 (2011).

[38] M. I. Dykman, "Large fluctuations and fluctuational transitions in systems driven by colored gaussian-noise: a high-frequency noise," Phys. Rev. A **42**, 2020–2029 (1990).

[39] M. I. Dykman, "Poisson-noise-induced escape from a metastable state," Phys. Rev. E **81**, 051124 (2010).

[40] R. P. Feynman and A. R. Hibbs, Quantum Mechanics and Path Integrals (McGraw-Hill, Inc., 1965).

[41] Throughout the paper, boldface lower-case letters will indicate vectors, while boldface upper-case letters will indicate matrices.

[42] W.H. Fleming and R.W. Rishel, Deterministic and stochastic optimal control (Springer New York, 1975).

[43] The vector multiplication here is assumed to be an inner product.

[44] Brandon S. Lindley and Ira B. Schwartz, "An iterative action minimizing method for computing optimal paths in stochastic dynamical systems," Physica D: Nonlinear Phenomena **255**, 22–30 (2013).

[45] Freddy Bouchet and Julien Reygner, "Generalisation of the eyring–kramers transition rate formula to irreversible diffusion processes," Annales Henri Poincaré **17**, 3499–3532 (2016).

[46] Klementyna Szwaykowska, Luis Mier-y-Teran Romero, and Ira B. Schwartz, "Collective Motions of Heterogeneous Swarms," IEEE Transactions on Automation Science and Engineering **12**, 810–arXiv:1409.1042.

[47] Lora Billings, Ira B. Schwartz, Marie McCrary, A. N. Korotkov, and Mark I. Dykman, "Switching Exponent Scaling near Bifurcation Points for Non-Gaussian Noise," Physical Review Letters **104**, 140601 (2010).

[48] Numerically, we introduced a large finite period to scale the integration to a unit arc length [44]. We have given examples show that a change in magnitude of the coupling may decrease the optimal force by three orders of magnitude.